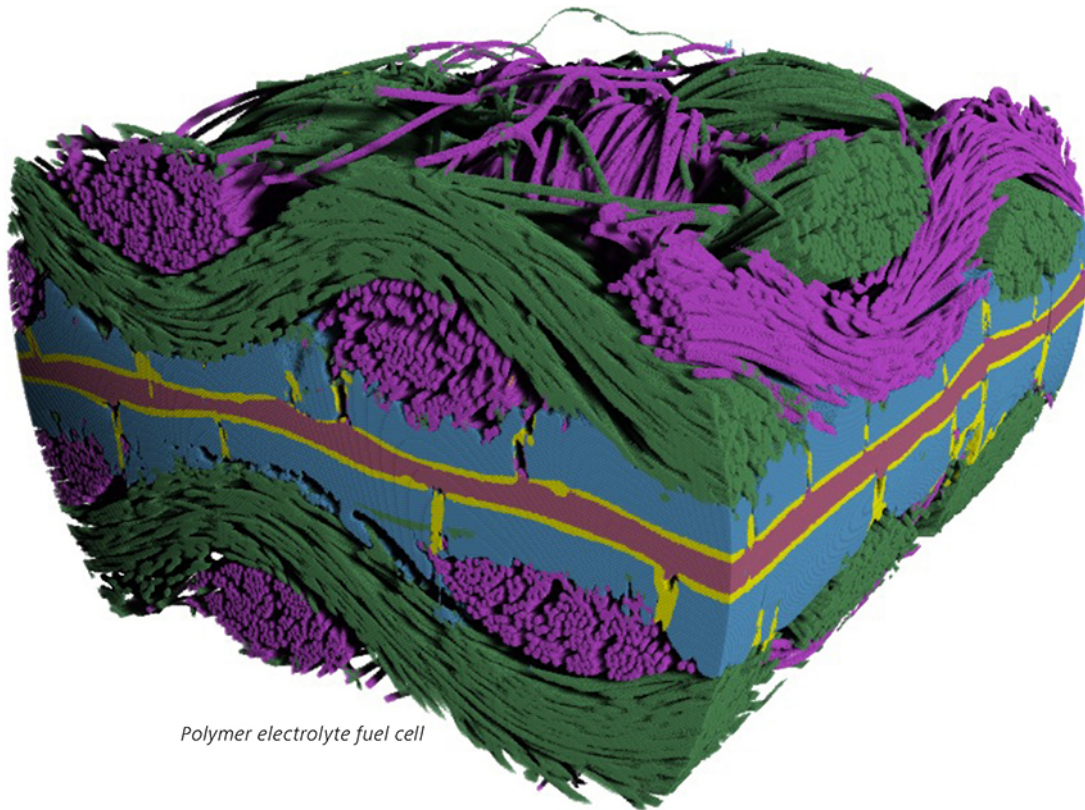


3D Characterization for Your 3D Material Structures.

- See even smaller sub-micron details
- Unprecedented image clarity at unprecedented speed enabled by AI
- UX designed for novices and experts alike



Polymer electrolyte fuel cell

Introducing ZEISS Xradia 630 Versa 3D X-ray Microscope

Seeing inside advanced materials can provide critical clues related to how structure affects performance. Achieving this insight at the microscale requires the clearest and highest-resolution 3D X-ray images. Use the newest ZEISS Xradia Versa 3D X-ray microscope (XRM) for nondestructive characterization of the finest sub-micron features within your materials. Leverage deep learning for the clearest 3D images across large representative volumes. Enjoy an intuitive, guided user experience that makes XRM technology accessible to all user skill levels.



Seeing beyond

Strong-Proton-Adsorption Co-Based Electrocatalysts Achieve Active and Stable Neutral Seawater Splitting

Ning Wang, Pengfei Ou, Sung-Fu Hung, Jianan Erick Huang, Adnan Ozden, Jehad Abed, Ivan Grigioni, Clark Chen, Rui Kai Miao, Yu Yan, Jinqiang Zhang, Ziyun Wang, Roham Dorakhan, Ahmed Badreldin, Ahmed Abdel-Wahab, David Sinton, Yongchang Liu, Hongyan Liang,* and Edward H. Sargent*

Direct electrolysis of pH-neutral seawater to generate hydrogen is an attractive approach for storing renewable energy. However, due to the anodic competition between the chlorine evolution and the oxygen evolution reaction (OER), direct seawater splitting suffers from a low current density and limited operating stability. Exploration of catalysts enabling an OER overpotential below the hypochlorite formation overpotential (≈ 490 mV) is critical to suppress the chloride evolution and facilitate seawater splitting. Here, a proton-adsorption-promoting strategy to increase the OER rate is reported, resulting in a promoted and more stable neutral seawater splitting. The best catalysts herein are strong-proton-adsorption (SPA) materials such as palladium-doped cobalt oxide ($\text{Co}_{3-x}\text{Pd}_x\text{O}_4$) catalysts. These achieve an OER overpotential of 370 mV at 10 mA cm^{-2} in pH-neutral simulated seawater, outperforming Co_3O_4 by a margin of 70 mV. $\text{Co}_{3-x}\text{Pd}_x\text{O}_4$ catalysts provide stable catalytic performance for 450 h at 200 mA cm^{-2} and 20 h at 1 A cm^{-2} in neutral seawater. Experimental studies and theoretical calculations suggest that the incorporation of SPA cations accelerates the rate-determining water dissociation step in neutral OER pathway, and control studies rule out the provision of additional OER sites as a main factor herein.

For practical seawater electrolysis, it will be essential to develop robust anode electrocatalysts that enable efficient and long-lasting oxygen evolution at high current densities.^[4]

Carrying out seawater electrolysis at high pH (>10) achieves suppression of the undesired chloride evolution reaction (CER).^[5] However, seawater electrolysis in alkaline electrolyte leads to the precipitation of magnesium and calcium salts at the cathode. Additionally, the consumption of lye and acid neutralizes the effluent stream, imposing added complexity and energy penalties to the process.^[6–8]

The direct electrolysis of seawater at near-neutral pH has the potential to avoid these challenges, while offering more favorable operating conditions for hybrid biological/electrochemical systems.^[8] At near-neutral conditions, the competing $2e^-$ transfer CER, which occurs due to the existence of chloride anions ($\approx 0.5 \text{ M}$ in seawater), competes with the oxygen evolution reaction (OER) above the 480 mV overpotential window.^[9,10]

This motivates ever-lower overpotentials in neutral OER. However, this is particularly challenging for near-neutral pH

1. Introduction

Seawater is an abundant natural resource and the topic of its electrolysis is one of interest in clean hydrogen production.^[1–3]

N. Wang, P. Ou, J. E. Huang, J. Abed, I. Grigioni, C. Chen, Y. Yan, J. Zhang, Z. Wang, R. Dorakhan, E. H. Sargent
Department of Electrical and Computer Engineering
University of Toronto
35 St George Street, Toronto, Ontario M5S 1A4, Canada
E-mail: ted.sargent@utoronto.ca

N. Wang, Y. Liu, H. Liang
School of Materials Science and Engineering and Key Laboratory of Efficient Utilization of Low and Medium Grade Energy
Ministry of Education
Tianjin University
Tianjin 300350, P. R. China
E-mail: hongyan.liang@tju.edu.cn

 The ORCID identification number(s) for the author(s) of this article can be found under <https://doi.org/10.1002/adma.202210057>.

DOI: 10.1002/adma.202210057

S.-F. Hung
Department of Applied Chemistry
National Yang Ming Chiao Tung University
Hsinchu 300, Taiwan

A. Ozden, R. K. Miao, D. Sinton
Department of Mechanical and Industrial Engineering
University of Toronto
5 King's College Road, Toronto, Ontario M5S 3G8, Canada

A. Badreldin, A. Abdel-Wahab
Chemical Engineering Program
Texas A&M University at Qatar
Doha 23874, Qatar

Y. Liu
State Key Lab of Hydraulic Engineering Simulation and Safety
Tianjin University
Tianjin 300350, P.R. China

operation since the reactant (OH^-) concentration in pH-neutral electrolytes is orders of magnitude lower than that in alkaline electrolytes.^[11,12] To date, oxygen evolution in pH neutral electrolytes has been observed with sub-480 mV overpotentials only at a low current density ($\leq 10 \text{ mA cm}^{-2}$) and with limited operating stability ($< 100 \text{ h}$).^[13–16]

Noting that pH-neutral electrolyte leads to a high overpotential due to the low concentration of OH^- arising due to the sluggish water dissociation step, prior researchers showed that optimizing hydroxide adsorption strength accelerates the water dissociation step and thus the hydrogen evolution reaction in non-acidic media.^[17,18]

We focused instead on the OER side of the reaction in pH-neutral media, seeking to provide strong proton adsorption on the electrocatalyst surface. We incorporate a series of strong proton adsorption (SPA) cations into the Co_3O_4 framework and find that the most active SPA-modified electrocatalyst, $\text{Co}_{3-x}\text{Pd}_x\text{O}_4$, enables a 370 mV overpotential at 10 mA cm^{-2} , decreasing the overpotential compared to pure Co-based catalysts by 70 mV. The catalyst maintains stable OER in

pH-neutral seawater for over 450 h at a constant current density of 200 mA cm^{-2} . Experimental studies and density functional theory (DFT) calculations reveal the synergetic effects between Co active sites and SPA cations: Co active sites adsorb OER intermediates, working in concert with SPA cations to favor the dissociation of water molecules, thus enhancing OER performance in neutral conditions.

2. Synthesis and Characterization of $\text{Co}_{3-x}\text{Pd}_x\text{O}_4$ Catalysts

To achieve the proposed proton-adsorption-promoting strategy in pH-neutral seawater oxidation reaction (Figure 1a), we firstly took advantage of electrochemical deposition to synthesize $\text{Co}_{3-x}\text{Pd}_x\text{O}_4$ catalysts on carbon paper. Scanning electron microscopy (SEM, Figure S1, Supporting Information) and transmission electron microscopy (TEM, Figure S2, Supporting Information) images reveal a nanoparticle morphology with rough and dense surface morphology. High-resolution TEM

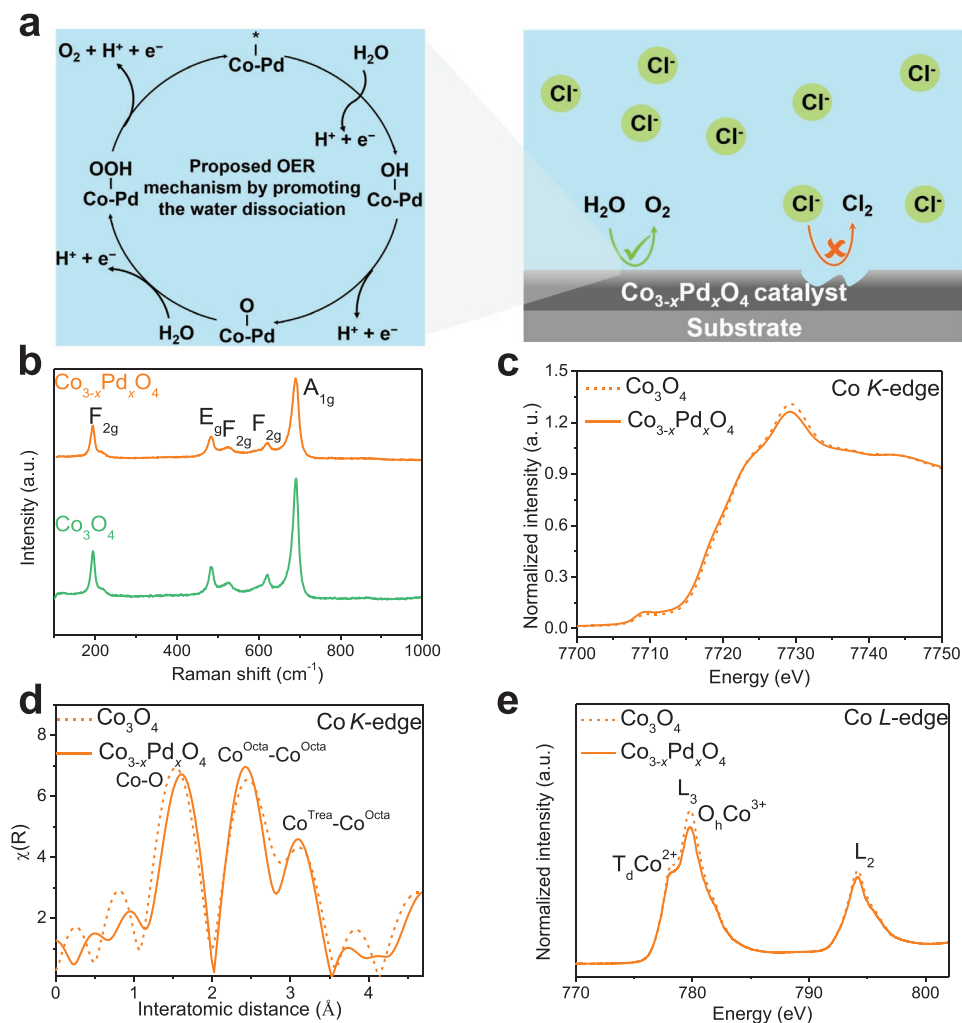


Figure 1. Proposed OER mechanism and structure characterization of electrodeposited $\text{Co}_{3-x}\text{Pd}_x\text{O}_4$ and controls. a) Proton-adsorption-promoting strategy in pH-neutral seawater oxidation reaction. b) Raman spectrum obtained using carbon paper substrates showing five characteristic peaks similar to Co_3O_4 . c) X-ray absorption and d) Fourier analysis of the EXAFS comparison at the Co K-edge in fluorescence mode. e) Co L-edge XAS spectra (acquired with soft X-ray excitation).

(HRTEM) images in Figure S2 (Supporting Information) revealed the nanocrystalline domains in both samples. These lattice fringe images reveal that the $\text{Co}_{3-x}\text{Pd}_x\text{O}_4$ catalyst (0.284 nm) shows a larger lattice distance than the Co_3O_4 catalyst (0.252 nm), consistent with Pd doping into the Co_3O_4 . Energy-dispersive X-ray spectroscopy (EDS) mapping in Figure S3 and S4, (Supporting Information) confirmed the successful introduction of Pd in Co_3O_4 . The substantially homogeneous distribution (within the technique spatial resolution) of Co, Pd, and O demonstrated the formation of a uniform oxide phase, without obvious impurity phase segregation. Using the inductively coupled plasma optical emission spectroscopy (ICP-OES), the atomic ratio of Co:Pd was determined to be 25:1, which is similar to the elemental ratio estimated by XPS collected from both the Ar plasma etched surface and the pristine surface (Figure S5, Supporting Information).

X-ray photoelectron spectroscopy (XPS) of Pd 3d and the X-ray absorption near-edge structure (XANES) spectrum of Pd *K*-edge spectrum suggest the incorporation of Pd into the Co_3O_4 with Pd valence +2 (Figure S6,S7, Supporting Information).^[19] The X-ray diffraction pattern and Raman spectrum of $\text{Co}_{3-x}\text{Pd}_x\text{O}_4$ shows no new peaks when one compares to those of the Co_3O_4 . This result suggests the absence of observable Pd phase segregation (Figure S8, Supporting Information, and Figure 1b).

To understand the effect of Pd on the local electronic structure of Co_3O_4 catalyst, we acquired ex situ and in situ spectra under the OER conditions. Co *K*- and *L*-edge X-ray absorption spectroscopy (XAS) reveal electronic structure changes in

$\text{Co}_{3-x}\text{Pd}_x\text{O}_4$ compared to in Co_3O_4 (Figure 1c–e, Figure S9, Supporting Information); these indicate that the incorporation of Pd cations affects the local electronic structure of Co. Incorporating Pd decreases the Co valence state (2.64 \rightarrow 2.46) and increases the Co–O bond distance. In situ XANES and EXAFS characterization and fitting show that the Co valence state and Co–O coordination number increases with applied potential, indicating that Co is active site and OER intermediates tend to adsorb on the Co active sites of the $\text{Co}_{3-x}\text{Pd}_x\text{O}_4$ catalyst (Figure S10,S11 and Table S1, Supporting Information), something also seen in DFT calculations.

3. Water Splitting Performance of $\text{Co}_{3-x}\text{Pd}_x\text{O}_4$ Catalysts

OER analysis was carried out in simulated seawater electrolyte (0.5 M NaCl and 1 M phosphate buffer solution). Linear scan voltammetry (LSV) curves show that $\text{Co}_{3-x}\text{Pd}_x\text{O}_4$ enables the lowest overpotential among members of the library of catalytic materials studied (Figure 2a, see Figure S12, Supporting Information, for cyclic voltammetry curves). The overpotential on $\text{Co}_{3-x}\text{Pd}_x\text{O}_4$ at a geometric current density of 10 mA cm⁻² is 370 \pm 2 mV, lower than that of Co_3O_4 and literature benchmark catalysts (437 \pm 2 mV,^[20] Figure S13 and Table S2, Supporting Information). We also compared the performance of the catalysts on planar Ti foil substrates and found a similar trend (Figure S14, Supporting Information). We further tested the catalytic performance of $\text{Co}_{3-x}\text{Pd}_x\text{O}_4$ catalyst with a range

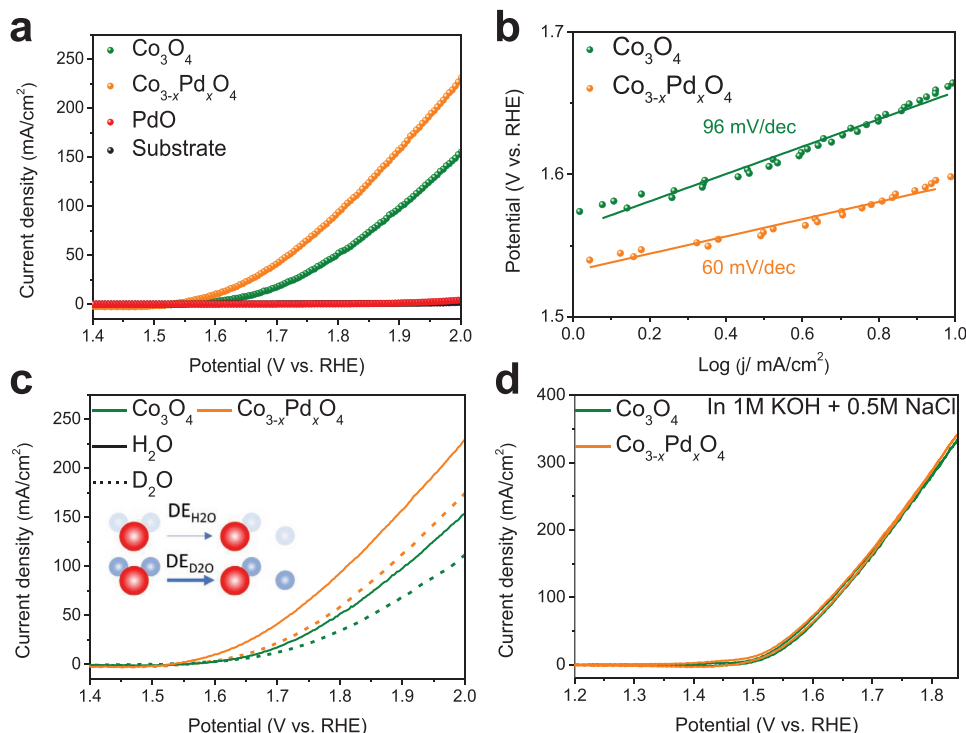


Figure 2. Catalytic performance comparison of electrodeposited $\text{Co}_{3-x}\text{Pd}_x\text{O}_4$ and controls at a scan rate of 1 mV s⁻¹ on carbon paper substrates in pH neutral simulated seawater (1 M PBS + 0.5 M NaCl). a, OER LSV polarization curves without iR correction. b) The corresponding Tafel slopes. c) LSV polarization performance obtained in H₂O and D₂O electrolytes. d) OER LSV polarization curves without iR correction in alkaline seawater electrolyte (1 M KOH + 0.5 M NaCl).

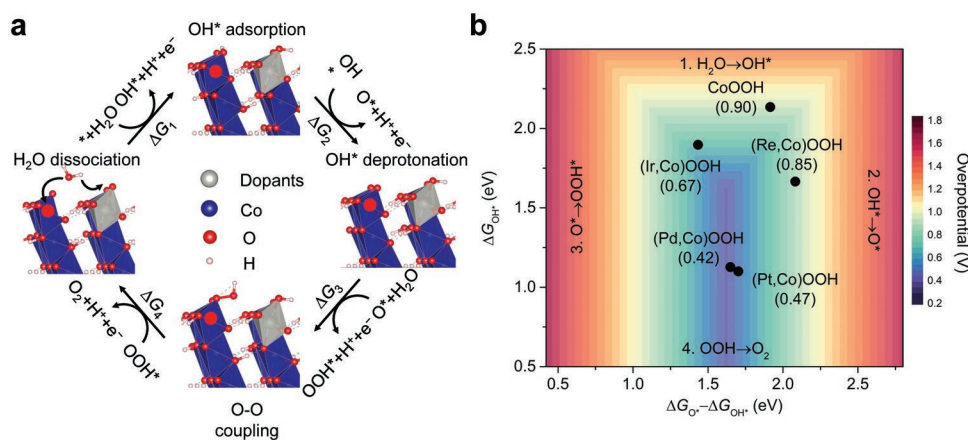


Figure 3. OER theoretical analysis. a) Proposed OER cycle of (Pd,Co)OOH by promoting the water dissociation assisted by adsorbed H* (cobalt, blue; palladium, grey; oxygen, red; hydrogen, pink). b) 2D OER activity map of theoretical overpotentials regarding different dopants in CoOOH (Pd, Ir, Pt, and Re) constructed by assuming a scaling relation $\Delta E_{\text{OOH}^*} = \Delta E_{\text{OH}^*} + 3.2 \text{ eV}$. G, Gibbs free energy. *, vacant site or adsorbed reaction intermediate.

of electrodeposition scan numbers to explore the effect of mass loading on catalytic performance. We obtained similar catalytic performance on the catalysts having various mass loadings, indicating that mass loading does not have a dominant impact on the optimization of OER performance (Figure S15, Supporting Information).

We also evaluated the intrinsic activity of $\text{Co}_{3-x}\text{Pd}_x\text{O}_4$ and Co_3O_4 catalysts by normalizing electrochemically active surface area (ECSA), determined with the aid of the double-layer capacitance (C_{dl}).^[21] The ECSA-normalized current density of $\text{Co}_{3-x}\text{Pd}_x\text{O}_4$ catalyst at 1.7 V versus RHE is $2.2\times$ higher than that of the Co_3O_4 catalysts (Figure S16, Supporting Information). Consistent with these findings, charge-transfer resistance (R_{ct}) determined using electrochemical impedance spectroscopy (EIS, Figure S17, Supporting Information) shows that incorporating Pd^{2+} decreases the R_{ct} from 68 to 15 Ω at the same potential (Figure S17 and Table S3, Supporting Information). The smaller iR -corrected overpotential in $\text{Co}_{3-x}\text{Pd}_x\text{O}_4$ catalysts gives evidence against a strong influence of cell geometry and conductivity on performance (Figure S18, Supporting Information). Turnover frequency (TOF) shows a similar trend: $\text{Co}_{3-x}\text{Pd}_x\text{O}_4$ catalysts exhibit a TOF of $0.18 \pm 0.03 \text{ s}^{-1}$ at 1.8 V versus RHE (TOF on Co_3O_4 catalyst is $0.11 \pm 0.02 \text{ s}^{-1}$, Table S4, Supporting Information).

We further tested the performance of $\text{Co}_{3-x}\text{Pd}_x\text{O}_4$ catalysts across a wide range of Pd concentrations. We report as a result the measured dependence of the catalytic performance of $\text{Co}_{3-x}\text{Pd}_x\text{O}_4$ as a function of Pd dopant concentration (Figure S19, Supporting Information). In situ Pd XAS spectra indicate no significant change in the electronic structure during the OER process (Figure S20, Supporting Information). These results suggest that Pd in Co_3O_4 assists the Co active sites to accelerate the OER kinetics, rather than providing additional OER sites.

Tafel slopes measured for OER on Co_3O_4 suggest that the water dissociation is the rate-determining step in a pH-neutral environment ($\approx 96 \pm 2 \text{ mV dec}^{-1}$).^[22,23] The Pd dopant ($\approx 60 \pm 3 \text{ mV dec}^{-1}$, Figure 2b) promotes OER kinetics,^[24,25] indicating that it lowers the energy barrier for water dissociation. We conducted water splitting reactions in deuterated water

(D_2O) under the same reaction conditions to evaluate the role of water dissociation. D_2O induces an increased overpotential compared to the corresponding values in H_2O (Figure 2c), and $\text{Co}_{3-x}\text{Pd}_x\text{O}_4$ catalyst shows a higher overpotential value change than control catalyst in D_2O ($46 \rightarrow 20 \text{ mV}$), consistent with the hypothesis that Pd plays a role in water dissociation.^[26,27]

To query whether the Pd-induced enhancement in OER activity is specific to pH neutral OER, we also studied alkaline seawater OER: when we worked at a high pH of ≈ 13.6 , we saw no significant difference in overpotential for $\text{Co}_{3-x}\text{Pd}_x\text{O}_4$ vs Co_3O_4 (Figure 2d). Since OH^- is abundant in alkaline OER, and the water dissociation step is not involved in OER,^[28–30] these ECSA and TOF studies obtained in alkaline seawater agree with the picture that the enhanced OER performance of $\text{Co}_{3-x}\text{Pd}_x\text{O}_4$ catalysts operating in neutral seawater originates from the accelerated water dissociation step (Figure S21 and Table S5, Supporting Information).

4. Density Functional Theory (DFT) Calculations

We carried out the DFT studies of the OER cycle on a $(01\bar{1}2)$ surface of Co oxyhydroxide (CoOOH)^[31] (see Materials and Methods for details). CoOOH is limited by dissociating water into $\text{H}^+ + \text{OH}^*$, suggesting that the first step, OH^* formation, is potential-determining with a theoretical overpotential of 0.90 eV, in agreement with a prior report.^[31] We then substitutionally doped CoOOH ($01\bar{1}2$) with Pd^{2+} and found that the water dissociation is promoted when the dissociated H is adsorbed on Pd dopants, i.e. it lowers the calculated overpotential (Figure S22, Supporting Information). Compared to CoOOH , the Gibbs free energy of OH^* formation on $(\text{Pd,Co})\text{OOH}$ is closer to 1.23 eV, rendering that the surface formation of O^* from OH^* becomes the potential-determining step (0.42 eV). We ascribed the changes both in the potential-determining step and theoretical overpotential to the transformation of the surface O-termination into an OH-termination arising from enhanced H^* adsorption functionality at the Pd site (Figure 3a), consistent with the experimental results.

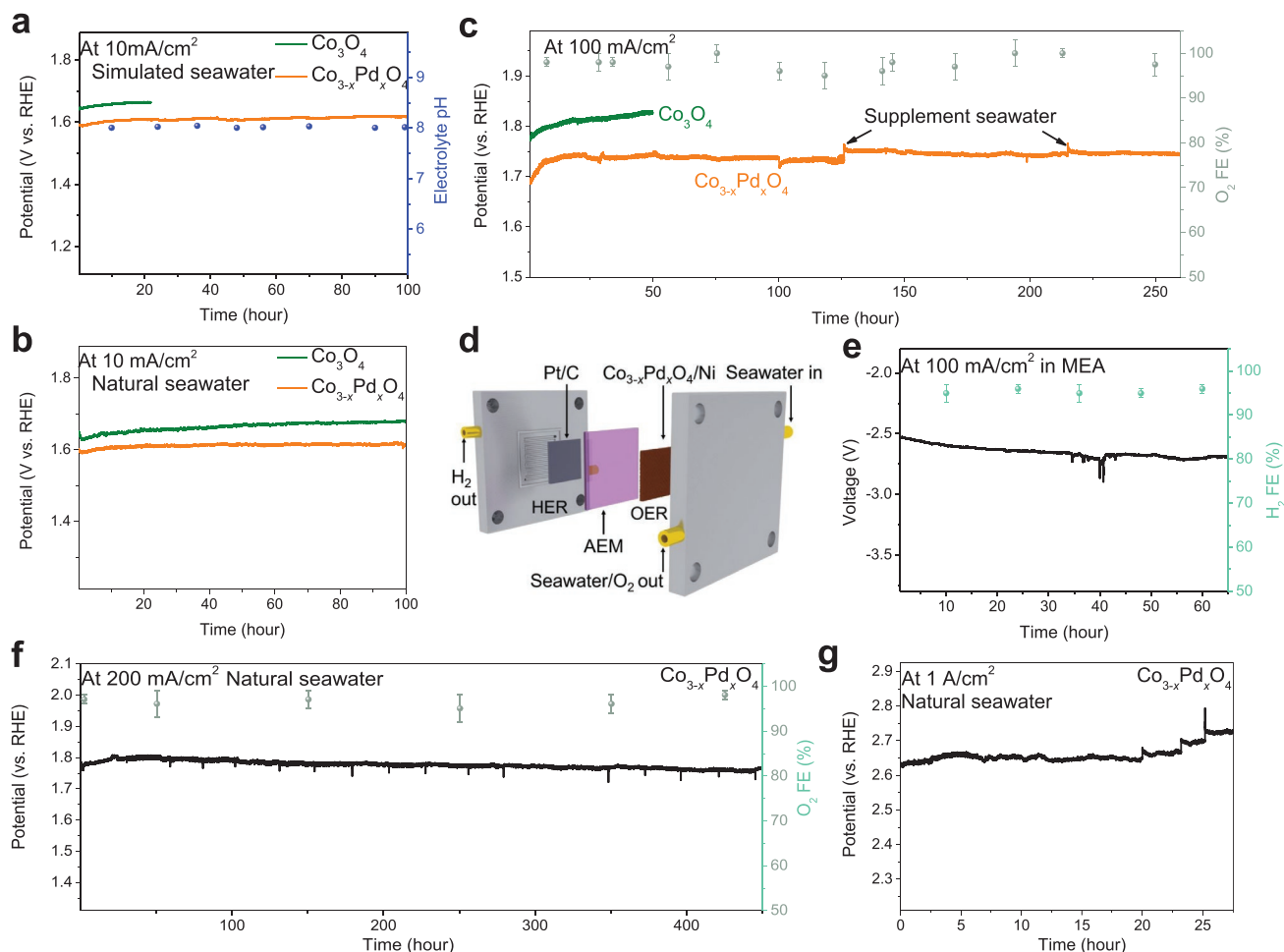


Figure 4. Seawater splitting stability test at different current density. a,b) Long-term stability test for the $\text{Co}_{3-x}\text{Pd}_x\text{O}_4$ and controls on carbon paper in simulated seawater (0.5 M NaCl and 1 M PBS) (a) and natural seawater electrolyte (seawater and 1 M PBS) (b), and the corresponding pH of the electrolyte. c) Stability tests comparison of $\text{Co}_{3-x}\text{Pd}_x\text{O}_4$ catalysts and controls on MnO_2 protected Ni foam substrates at a current density of 100 mA cm^{-1} in natural seawater electrolyte, and the corresponding O_2 FE from GC measurement. d) MEA system structure. $\text{Co}_{3-x}\text{Pd}_x\text{O}_4$ supported on MnO_2 protected Ni foam used as the anode. The Pt-C catalyst on hydrophobic carbon paper acted as cathode. Humidified N_2 was flowed through the gas channels in the cathode, and natural seawater electrolyte was flowed through channels in the anode. e) Operating voltage and H_2 FE were monitored at constant 100 mA cm^{-2} in a MEA device. f,g) Stability tests of $\text{Co}_{3-x}\text{Pd}_x\text{O}_4$ catalysts on MnO_2 protected Ni foam substrates at current densities of 200 mA cm^{-2} (f) and 1 A cm^{-2} (g) in natural seawater electrolyte.

We extended the model of $(\text{Pd},\text{Co})\text{OOH}$ to other dopants with SPA capability (Ir, Pt, and Re),^[32] where we sought to employ the same doping site and surface termination groups. The SPA dopants are predicted to have lower theoretical overpotentials compared to pristine CoOOH : the calculated theoretical overpotential follows the trend $(\text{Pd},\text{Co})\text{OOH} < (\text{Pt},\text{Co})\text{OOH} < (\text{Ir},\text{Co})\text{OOH} < (\text{Re},\text{Co})\text{OOH} \approx \text{CoOOH}$ (Figure 3b). This finding agrees well with experimental trends (Figure S23,S24, Supporting Information), with Pd the best among the dopants screened.

5. Seawater Splitting: Operating Stability

To investigate the feasibility of neutral seawater electrolysis using $\text{Co}_{3-x}\text{Pd}_x\text{O}_4$ catalysts, we performed electrocatalytic measurements in simulated seawater (1 M phosphate buffer solution + 0.5 M NaCl) and natural seawater solution

(1 M phosphate buffer solution + natural seawater from the Barnet Marine Beach, Vancouver). We firstly tested performance in simulated seawater for 100 h and saw no significant change in potential and bulk pH (Figure 4a; Figure S25, Supporting Information). O-Tolidine was used to test for hypochlorite/hypochlorous acid in the electrolyte following long-term seawater electrolysis.^[16] We detected no color change in $\text{Co}_{3-x}\text{Pd}_x\text{O}_4$ catalyst (Figure S26, Supporting Information). In natural seawater, the $\text{Co}_{3-x}\text{Pd}_x\text{O}_4$ catalyst was also stable upon continuous operation for $\approx 100 \text{ h}$ at 10 mA cm^{-2} (Figure 4b). UV-vis spectra^[33] of the $\text{Co}_{3-x}\text{Pd}_x\text{O}_4$ indicate hypochlorite concentration $\leq 1.5 \mu\text{mol L}^{-1}$, $16\times$ lower than in the case of Co_3O_4 (Figure S27,S28, Supporting Information).

To avoid Cl^- corrosion to the Ni foam substrate, we introduced MnO_2 on top of the substrate as a protective layer^[34] (Figure S29,S30, Supporting Information). The $\text{Co}_{3-x}\text{Pd}_x\text{O}_4$ catalyst deposited on the modified substrate operated continuously

for 250 hours without a change in potential at 100 mA cm⁻² in natural seawater (Figure 4c). The resulting gas chromatography (GC) spectra showed a $\approx 97 \pm 2\%$ oxygen Faradaic efficiency (FE) on the Co_{3-x}Pd_xO₄ catalyst, indicating selective OER in pH neutral seawater. Over the course of 250 h, the concentration of hypochlorite in seawater electrolyte was 8.3 $\mu\text{mol L}^{-1}$ (Figure S31, Supporting Information). We found that the structural, morphological, and compositional features of Co_{3-x}Pd_xO₄ catalyst were maintained during extended OER operation (Figure S32 and S33, Supporting Information). The ICP elemental ratio of Co:Pd of 24:1 is similar to the pre-OER value.

To investigate further the catalyst's viability in practical systems, we implemented Co_{3-x}Pd_xO₄ as the OER catalyst in a membrane electrode assembly (MEA) electrolyser that produces H₂ from seawater (Figure 4d). The electrolyser exhibited stable performance at 100 mA cm⁻² for over 65 h: it maintained a cell potential of -2.65 V and H₂ FE of 95 $\pm 2\%$ (Figure 4e).

We investigated the stability of Co_{3-x}Pd_xO₄ OER catalyst at higher current densities in natural seawater. We found that Co_{3-x}Pd_xO₄ catalysts maintain their seawater splitting performance over the course of 450 h at 0.2 A cm⁻² and 20 h at 1 A cm⁻² (Figure 4f,g).

Taken together, the experimental findings and DFT suggest that incorporating SPA cations into a Co-based oxide framework to form Co_{3-x}M_xO₄ catalysts achieves increased water dissociation that enhances OER performance in pH neutral seawater electrolytes, offering progress on the path to direct seawater utilization.

Supporting Information

Supporting Information is available from the Wiley Online Library or from the author.

Acknowledgements

N.W., P.O., S.-F.H. contributed equally to this work. The authors acknowledge funding from the Natural Gas Innovation Fund, the Natural Sciences and Engineering Research Council (NSERC) of Canada, Qatar National Research Fund under its National Priorities Research Program award number NPRP12S-0131-190024, Shell Global Solutions International B.V., and the Ontario Research Fund – Research Excellence program. All DFT computations were performed on the Niagara supercomputer of the SciNet HPC Consortium. SciNet was funded by the Canada Foundation for Innovation, the Government of Ontario, the Ontario Research Fund Research Excellence Program, and the University of Toronto. N.W. and H.L. acknowledge support from the National Natural Science Foundation of China (NSFC No. 51771132) and the Thousand Youth Talents Plan of China. The authors thank S.-F.H. for XAS technical support in NSRRC. S.-F.H. acknowledges support from the MOST funding (Contract No. MOST 110-2113-M-009-007-MY2). The authors thank Daniel Esposito for helpful discussions and suggestions.

Conflict of Interest

The authors declare no conflict of interest.

Author Contributions

E.H.S. and H.L. supervised the project. N.W. conceived the idea and carried out the experiments. N.W. P.O. and E.H.S. co-wrote the paper. P.O. carried out the DFT calculations. S.-F.H. conducted the in situ XAS, SRXRD, SEM, and TEM measurements. I.G., Y.Y., and J.E.H. assisted in electrochemical experiments. A.O. did the MEA test. A.O., J.A., J.E.H. S.-F.H., and C.C. assisted in data analysis, manuscript writing and polishing. All authors discussed the results and assisted during manuscript preparation.

Data Availability Statement

The data supporting this study are available in the paper and the Supplementary Information. All other relevant source data are available from the corresponding authors upon reasonable request.

Keywords

cobalt oxide, neutral seawater splitting, oxygen evolution reaction, strong-proton-adsorption effect

Received: October 31, 2022

Revised: January 21, 2023

Published online:

- [1] W. J. Jiang, T. Tang, Y. Zhang, J. S. Hu, *Acc. Chem. Res.* **2020**, *53*, 1111.
- [2] Z. Kato, M. Sato, Y. Sasaki, K. Izumiya, N. Kumagai, K. Hashimoto, *Electrochim. Acta* **2014**, *116*, 152.
- [3] F. Dionigi, T. Reier, Z. Pawolek, M. Gliech, P. Strasser, *ChemSusChem* **2016**, *9*, 962.
- [4] L. Yu, Q. Zhu, S. Song, B. McElhenny, D. Wang, C. Wu, Z. Qin, J. Bao, Y. Yu, S. Chen, Z. Ren, *Nat. Commun.* **2019**, *10*, 5106.
- [5] Y. Kuang, M. J. Kenney, Y. Meng, W. H. Hung, Y. Liu, J. E. Huang, R. Prasanna, P. Li, Y. Li, L. Wang, M.-C. Lin, M. D. McGehee, X. M. Sun, H. Dai, *Proc. Natl. Acad. Sci. USA* **2019**, *116*, 6624.
- [6] S. Dresp, F. Dionigi, M. Klingenhof, P. Strasser, *ACS Energy Lett.* **2019**, *4*, 933.
- [7] W. Tong, M. Forster, F. Dionigi, S. Dresp, R. Sadeghi Erami, P. Strasser, A. J. Cowan, P. Farràs, *Nat. Energy* **2020**, *5*, 367.
- [8] A. A. Bhardwaj, J. G. Vos, M. E. S. Beatty, A. F. Baxter, T. M. Koper, N. Y. Yip, D. V. Esposito, *ACS Catal.* **2021**, *11*, 1316.
- [9] S. Dresp, F. Dionigi, S. Loos, J. Ferreira de Araujo, C. Spöri, M. Gliech, H. Dau, P. Strasser, *Adv. Energy Mater.* **2018**, *8*, 1800338.
- [10] J. G. Vos, M. T. M. Koper, *J. Electroanal. Chem.* **2018**, *819*, 260.
- [11] K. Xu, H. Cheng, L. Liu, H. Lv, X. Wu, C. Wu, Y. Xie, *Nano Lett.* **2017**, *17*, 578.
- [12] N. Wang, Z. Cao, X. Zheng, B. Zhang, S. M. Kozlov, P. Chen, C. Zou, X. Kong, Y. Wen, M. Liu, Y. Zhou, C. T. Dinh, L. Zheng, H. Peng, Y. Zhao, L. Cavallo, X. Zhang, E. H. Sargent, *Adv. Mater.* **2020**, *32*, 1906806.
- [13] F. Cheng, X. Feng, X. Chen, W. Lin, J. Rong, W. Yang, *Electrochim. Acta* **2017**, *251*, 336.
- [14] J. Zheng, *Appl. Surf. Sci.* **2017**, *413*, 72.
- [15] P. Gayen, S. Saha, V. Ramani, *ACS Appl. Energy Mater.* **2020**, *3*, 3978.
- [16] S. H. Hsu, J. Miao, L. Zhang, J. Gao, H. Wang, H. Tao, S. F. Hung, A. Vasileff, S. Z. Qiao, B. Liu, *Adv. Mater.* **2018**, *30*, 1707261.
- [17] I. T. McCrum, M. T. M. Koper, *Nat. Energy* **2020**, *5*, 891.
- [18] C.-T. Dinh, A. Jain, F. P. G. de Arquer, P. De Luna, J. Li, N. Wang, X. Zheng, J. Cai, B. Z. Gregory, O. Voznyy, B. Zhang, M. Liu, D. Sinton, E. J. Crumlin, E. H. Sargent, *Nat. Energy* **2018**, *4*, 107.

- [19] S. Guo, G. Zhang, Z.-K. Han, S. Zhang, D. Sarker, W. W. Xu, X. Pan, G. Li, A. Baiker, *ACS Appl. Mater. Interfaces* **2020**, *13*, 622.
- [20] Y. Zhao, B. Jin, Y. Zheng, H. Jin, Y. Jiao, S.-Z. Qiao, *Adv. Energy Mater.* **2018**, *8*, 1801926.
- [21] H. Li, S. Chen, X. Jia, B. Xu, H. Lin, H. Yang, L. Song, X. Wang, *Nat. Commun.* **2017**, *8*, 15377.
- [22] L. M. D. Silva, J. F. C. Boodts, L. A. D. Faria, *Electrochim. Acta* **2001**, *46*, 1369.
- [23] Y.-H. Fang, Z.-P. Liu, *J. Am. Chem. Soc.* **2010**, *132*, 18214.
- [24] J. M. Hu, J. Q. Zhang, C. N. Cao, *Int. J. Hydrogen Energy* **2004**, *29*, 791.
- [25] E. Fabbri, A. Habereeder, K. Waltar, R. Kötz, T. J. Schmidt, *Catal. Sci. & Technol.* **2014**, *4*, 3800.
- [26] L. C. S. Melander, W. H. Saunders, Wiley, New York, 126 (Book, **1980**).
- [27] Z. Zhao, R. Bababrik, W. Xue, Y. Li, N. M. Briggs, D.-T. Nguyen, U. Nguyen, S. P. Crossley, S. Wang, B. Wang, D. E. Resasco, *Nat. Catal.* **2019**, *5*, 431.
- [28] H. Dau, C. Limberg, T. Reier, M. Risch, S. Roggan, P. Strasser, *ChemCatChem* **2010**, *2*, 724.
- [29] N. T. Suen, S. F. Hung, Q. Quan, N. Zhang, Y. J. Xu, H. M. Chen, *Chem. Soc. Rev.* **2017**, *46*, 337.
- [30] H. Y. Wang, S. F. Hung, H. Y. Chen, T. S. Chan, H. M. Chen, B. Liu, *J. Am. Chem. Soc.* **2016**, *138*, 36.
- [31] M. Bajdich, M. Garcia-Mota, A. Vojvodic, J. K. Nørskov, A. T. Bell, *J. Am. Chem. Soc.* **2013**, *135*, 13521.
- [32] J. Li, J. Hu, M. Zhang, W. Gou, S. Zhang, Z. Chen, Y. Qu, Y. Ma, *Nat. Commun.* **2021**, *12*, 1.
- [33] T. Kuwana, J. W. Strojek, *Discuss. Faraday Soc.* **1968**, *45*, 134.
- [34] J. G. Vos, T. A. Wezendonk, A. W. Jeremiasse, M. T. M. Koper, *J. Am. Chem. Soc.* **2018**, *140*, 10270.